Chapter 3

Beam-Beam Interactions

3.1 Introduction

As Chapter 2 has shown, a beam separation scheme with a relatively large crossing angle (2×11 mrad) has been chosen for KEKB. The expected benefits are as follows:

1. It makes it possible to accommodate a wide range of combinations of the bunch intensity vs. bunch spacing (minimum 0.6 m).

2. It makes it possible to use superconducting final focusing quadrupole magnets, and the system can provide collisions at $E_{CM} = 10.4 \sim 11.0$ GeV without modifying the hardware layout of the beam line.

3. The absence of separation bend magnets leads to a significant reduction of synchrotron radiation near the interaction point.

4. Compensation solenoid magnets can be implemented near the interaction point.

5. An extremely large beam separation is provided, even at the first parasitic collision point.

How this scheme is realistically adequate at KEKB depends on whether the behavior of the beams should be stable and satisfactory under finite angle crossing. The purpose of this chapter is to document the results of studies that have been carried out for KEKB in an effort to answer this question.

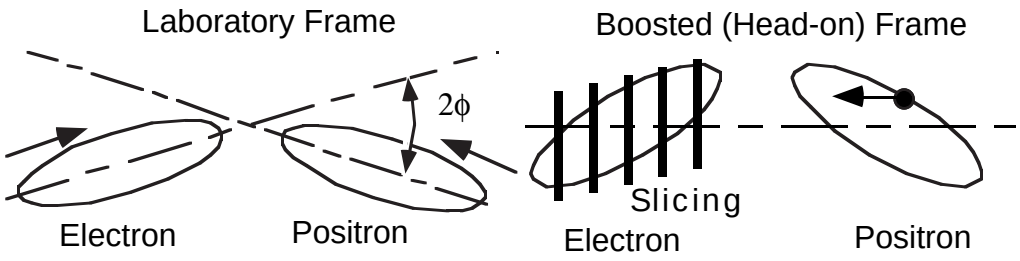

Figure 3.1: Lorentz transformation from the laboratory frame to the "head-on" frame, which is used for applying synchro-beam mapping to calculate beam-beam interactions with finite crossing angles.

3.2 Simulation of a Beam Collision with Finite Crossing Angles

A new modelling algorithm has been developed to simulate beam-beam collisions under finite crossing angles. In the algorithm, as indicated in Figure 3.1, the bunches that are colliding at the crossing angle are first Lorentz-transformed into a frame in which their momentum vectors are parallel. In this "head-on" frame a symplectic synchro-beam mapping is applied, and the beam-beam forces and their effects on the bunches are calculated. When the mapping is finished, the two bunches are Lorentz-transformed back to the laboratory frame, where the beam tracking code takes over the rest of the simulation.

This beam-beam code incorporates all known effects, including: (a) the energy loss due to the fact that a particle traverses the transverse electric fields at an angle, (b) energy loss due to longitudinal electric fields, and (c) effects due to the variation of β along the bunch length during a collision (hourglass effect).

Full descriptions of this code and its preliminary results are given in [1] and the references therein. To date, this is the only code known to us to be fully symplectic in the 6-dimensional phase space with the hourglass and crossing angle effects taken into account. The symplecticity in the 3-dimensional sense, and correct treatment of Lorentz-covariance and bunch slicing there are considered to be important in our application. This is because the planned total crossing angle (22 mrad) is comparable to the geometric angle of bunches at the IP of KEKB, *i.e.* $\sigma_x/\sigma_z = 19$ mrad.

3.3 Beam-Beam Simulation with Linear Lattice Functions

A series of beam-beam simulations has been conducted based on a simplified lattice model, where the beam transfer through the ring is represented by a one-turn matrix and a diffusion matrix [5]. Although the interaction between the beam-beam and non-linear lattice effects cannot be studied using this method, it allows us to quickly compare the luminosity performance in various beam parameter and tune conditions. This simulation is also necessary to compare the luminosity between linear and non-linear lattices.

In this simulation the beam-beam effect is calculated according to the prescriptions given in the previous section. A weak-strong formalism is used. Typically the strong bunch is longitudinally sliced in 5 slices, and the weak bunch is represented by 50 super-particles. The effects of radiation damping and diffusion are included in the calculation. Its details are given in [1]. Parameters such as the initial beam emittance, coupling, bunch intensity, β^*, orbit errors at the IP and the machine tunes are specified as initial conditions. Then, the beam-beam collision and revolutions through the ring are simulated for up to 10 radiation damping times. The resultant beam size is examined. The strong beam is given a specified Gaussian distribution. The weak beam has a distribution function given as the sum of δ-functions, which represent the ensemble of particles. The expected luminosity is calculated as a convolution of the distribution functions of the two beams.

The initial beam parameters in the simulation are specified in such a way that they would give the design luminosity value of 1×10^{34} cm^{2}s^{-1} or somewhat higher values, with collisions of 5120 bunches per ring in the absence of aberrations and beam blow-up. Figure 3.2 shows an example of the results from this simulation. In this case, the crossing angle at the IP is set to zero. The synchrotron tune ν_s is assumed to be 0.017. The figure shows a contour diagram of the expected luminosity as a function of the transverse tune (ν_x and ν_y) in the range $0 < \nu_x, \nu_y < 0.25$. The contour spacing is 10^{33} cm^{-2}s^{-1}. Pronounced luminosity reduction due to the coupling resonance is seen. Also, traces of $\nu_y = 2\nu_x$, $4\nu_x + 2\nu_y = 1$ and the synchro-betatron resonance $\nu_s = 2\nu_y$ are seen.

Figure 3.3 shows a similar luminosity contour plot in the ν_x-ν_y plane, but for the case with a crossing angle of 2×10 mrad. The beam intensity was changed from that of Figure 3.2 in order to adjust the geometric luminosity, while keeping the other parameters unchanged. An additional luminosity reduction due to the synchro-betatron resonance line $\nu_s = 2\nu_x$ is evident. Also, resonance lines such as $\nu_x = 2\nu_y$, $3\nu_x = 5\nu_y$,

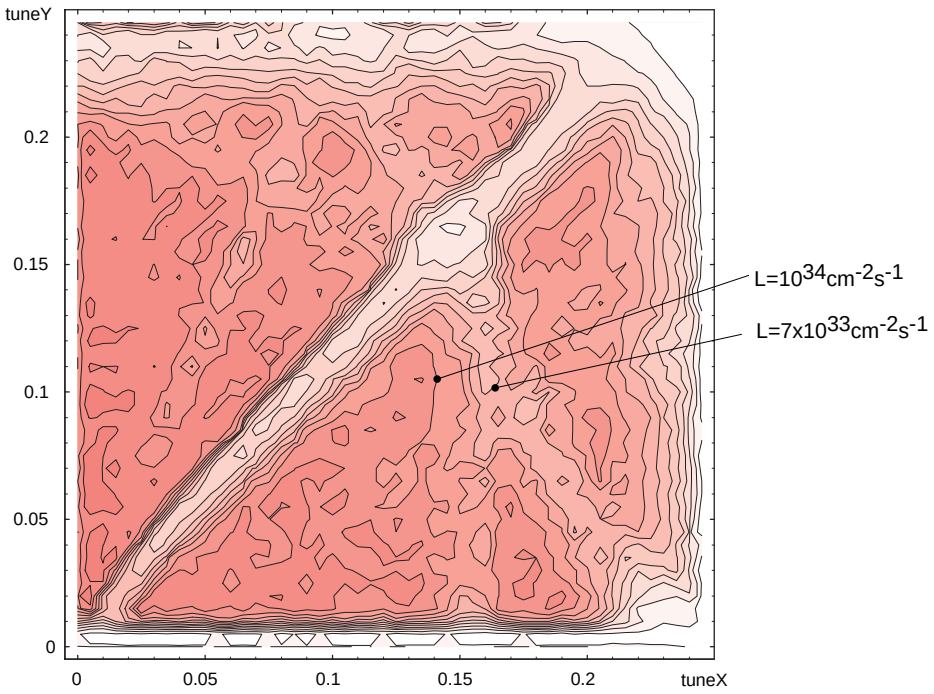

Figure 3.2: Result from a beam-beam simulation with a linear lattice model. In this case, the crossing angle is set to zero. The expected luminosity in the ν_x-ν_y plane is shown. The contour spacing is 10^{33} cm^{-2}s^{-1}.

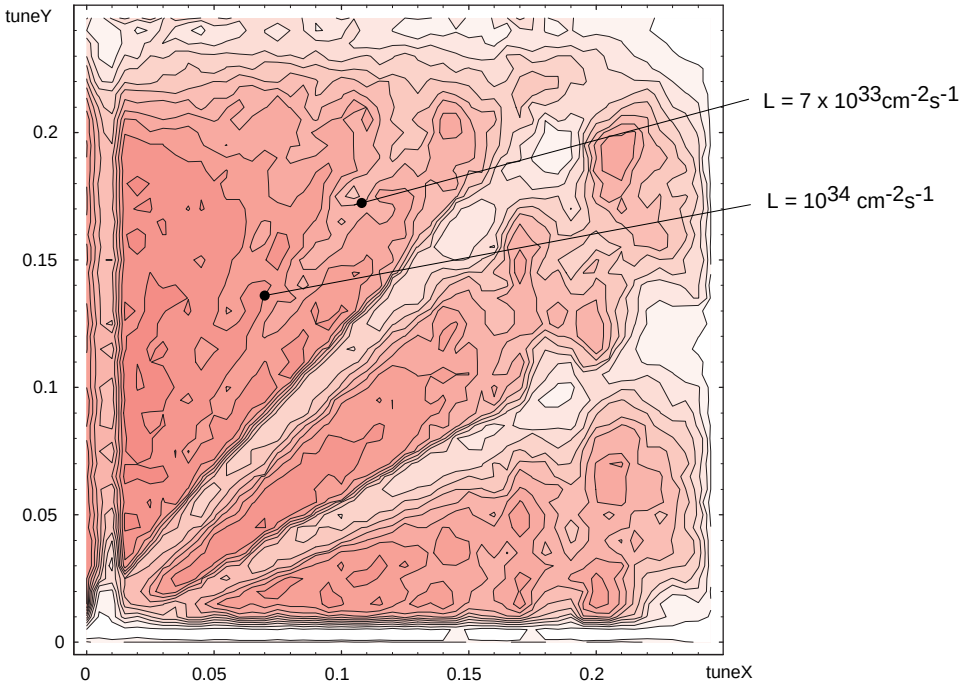

Figure 3.3: Calculated luminosity contour diagram in the case of a crossing angle of 2×10 mrad. The expected luminosity in the ν_x-ν_y plane is shown. The contour spacing is 10^{33} cm^{-2}s^{-1}.

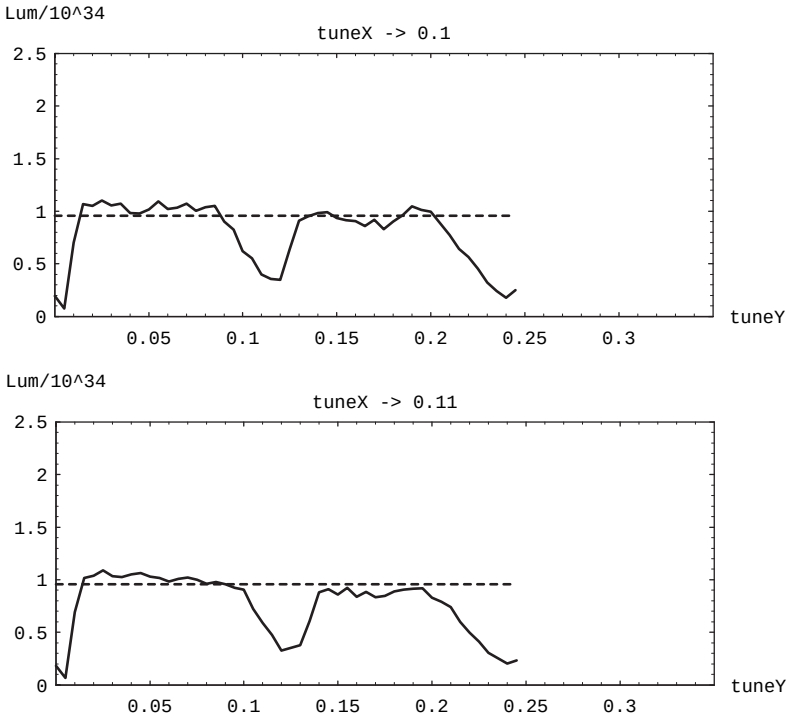

Figure 3.4: Two slices from the luminosity contour plot for the zero crossing angle case. The expected luminosity as a function of ν_y is shown for $\nu_x = 0.1$ and 0.11.

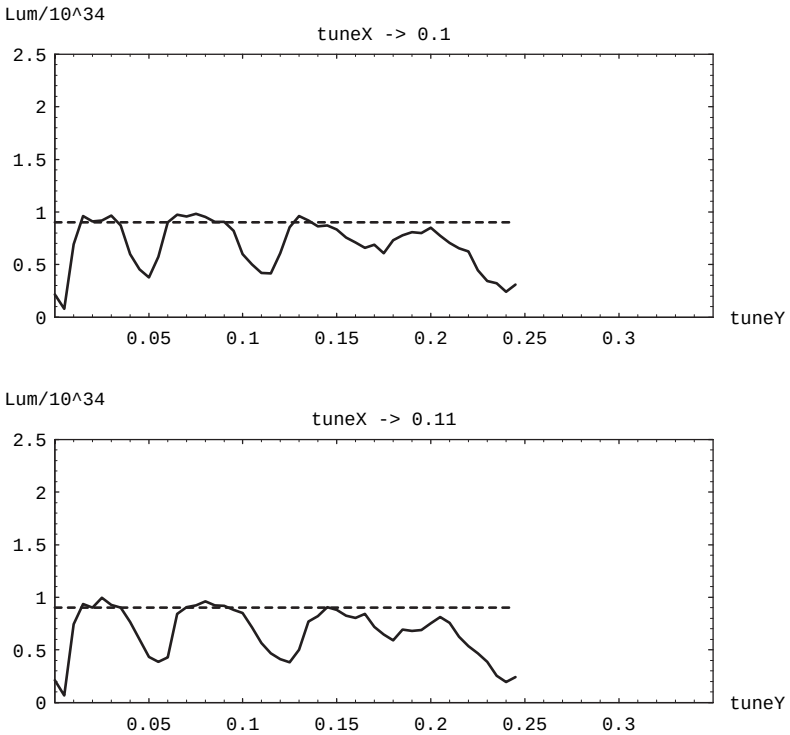

Figure 3.5: Two slices from the luminosity contour plot for a crossing angle of 2×10 mrad. The expected luminosity as a function of ν_y is shown for $\nu_x = 0.1$ and 0.11.

$3\nu_x = \nu_y$, and $4\nu_y - 4\nu_s = 1$ are causing a luminosity reduction. Those resonances did not cause a luminosity reduction in the case of the zero crossing angle. However, a sizeable amount of areas in the ν_x-ν_y plane appear to be intact.

Figure 3.4 shows two slices of the contour plot in Figure 3.2. The expected luminosity as a function of ν_y is shown for $\nu_x = 0.1$ and 0.11. Likewise, Figure 3.5 shows two slices of Figure 3.3 for a comparison.

Some notable observations are summarized as follows:

1. Introducing a finite crossing angle at the IP certainly causes a reduction of usable ν_x-ν_y combinations, because of synchro-betatron and other resonances. The effects are larger for a larger synchrotron tune ν_s, particularly when $\nu_s > 0.03$ holds.

2. However, when ν_s is kept small *i.e.* below 0.02, a fair amount of regions in the ν_x-ν_y plane is still free from synchro-betatron resonances, and thus they appear to be usable. Such regions exist as well-connected zones, rather than many isolated islands. Some of the acceptable ν_x-ν_y regions are compatible with the conditions preferred in dynamic aperture considerations.

3. For the beam intensity of a few $\times 10^{10}$ per bunch or below, no intensity-dependent beam blow-up is predicted with finite crossing angles, as far as this simulation using the simplified lattice model is concerned.

4. When the synchrotron tune (ν_s) is small, and when a resonance-free condition of ν_x-ν_y is chosen, the expected luminosity there is roughly consistent with naive expectations based on the geometric and linear effects, as discussed in Chapter 2.

5. The luminosity calculated with an ideal linear lattice, in some cases, can become larger than a naive expectation, which only considers geometric factors. This is because of effects of the dynamic beta [3] and dynamic emittance [4]. As an example, Figure 3.6 shows correction factors for the β and ϵ calculated for $0 < \nu_y < 0.1$.

The results from this study have been reviewed in conjunction with investigations on the tune-dependence of the dynamic aperture and other aspects of the KEKB design. It has been found that beam dynamics considerations in the lattice design favor a horizontal tune (ν_x) slightly above the half integer resonance. From studies on the engineering design required for magnets in the interaction region, a crossing angle of 2×11 mrad has been chosen. Figures 3.7 and 3.8 show the calculated luminosity tune

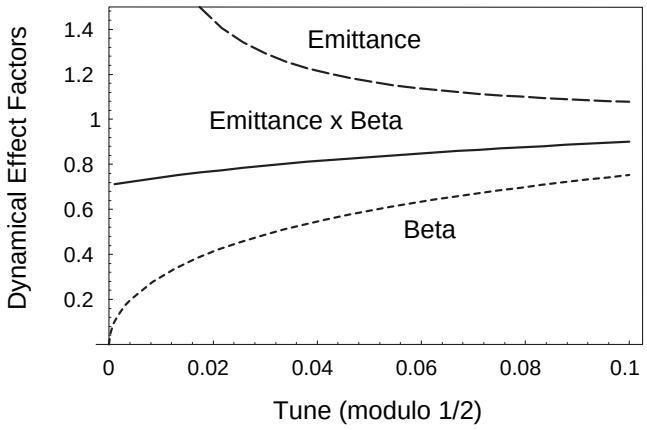

Figure 3.6: Dynamic beta and dynamic emittance effects: the dotted line indicates β, dashed line is ϵ and the solid line is $\beta\epsilon$. The horizontal axis is the tune (modulo 1/2). All of these are normalized by their nominal values.

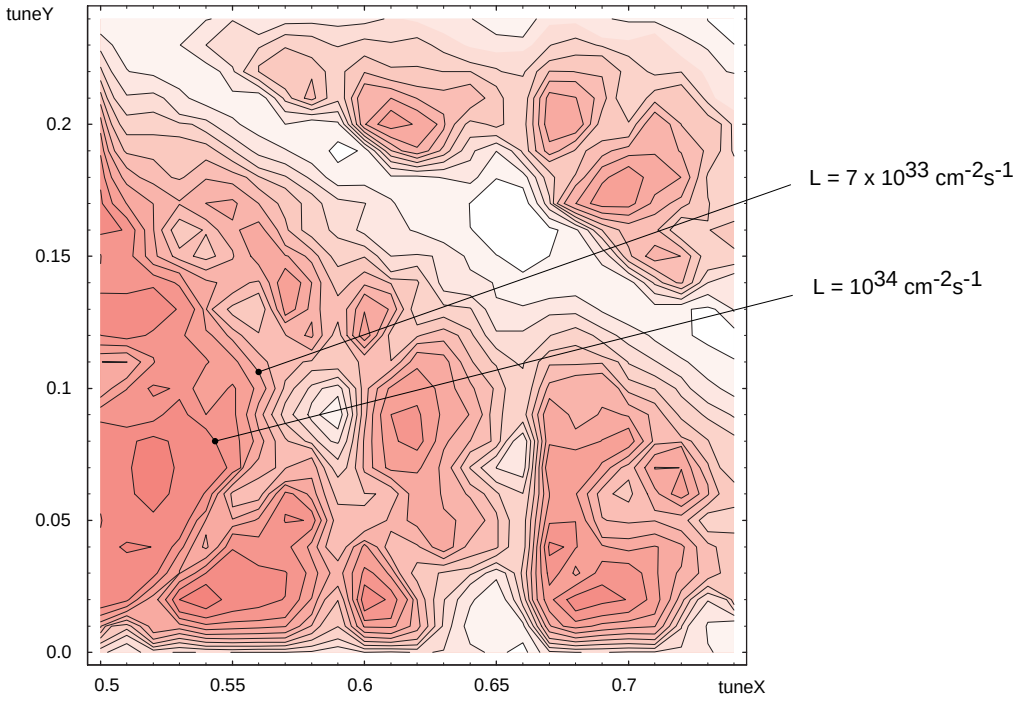

Figure 3.7: Result from a beam-beam simulation with simplified particle tracking. In this case, the crossing angle is set to 2×10 mrad. The expected luminosity in the ν_x-ν_y plane is shown. The contour spacing is 10^{33} cm^{-2}s^{-1}.

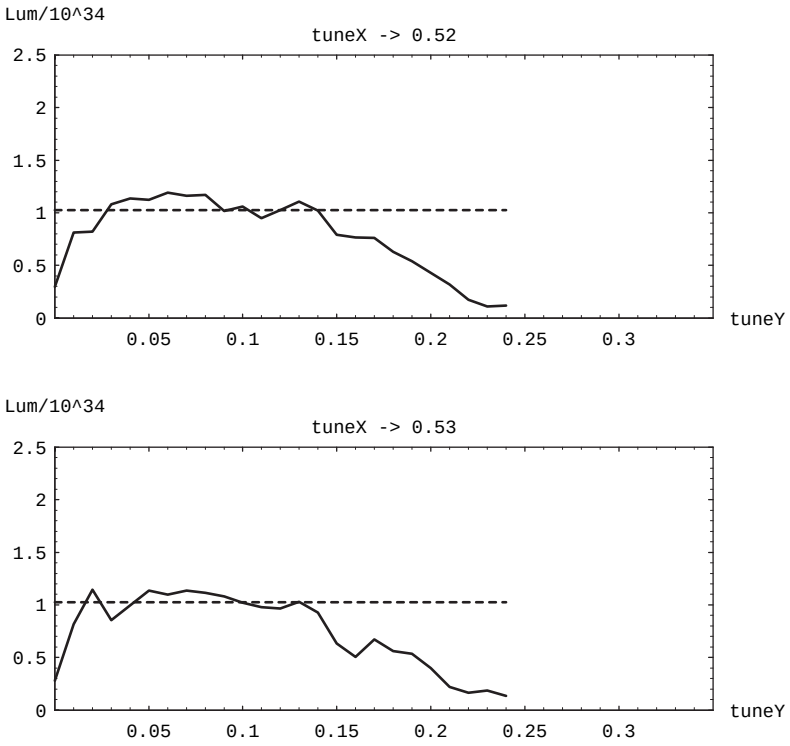

Figure 3.8: Two slices from the luminosity contour plot of for the region $0.5 < \nu_x < 0.75$ and $0 < \nu_y < 0.25$ as shown in Figure 3.7. Expected luminosity as function of ν_y is shown for $\nu_x = 0.52$ and 0.53.

diagram for $0.5 < \nu_x < 0.75$ and $0 < \nu_y < 0.25$. The final working parameters for the detailed design work have been determined as Table 3.1. The effective beam-beam parameter for this set of parameters is $\xi_{x,y} = (0.04, 0.05)$, which takes account of the dynamical reduction factors, as discussed in Chapter 1. Figure 3.9 shows the luminosity tune diagram, which gives a magnified view of the vicinity of the working parameter set.

Surveys have also been made on how the luminosity is affected by the bunch length. Let us call the bunch length of the weak beam σ_z^w and that of the strong beam σ_z^s. Figure 3.10 shows the expected luminosity as a function of σ_z^w and σ_z^s. The plot on the right side shows the expected luminosity (solid line) when the condition $\sigma_z^w = \sigma_z^s$ is imposed. The broken line in the plot shows the luminosity expected from a consideration of only the geometry. It is seen that a shorter bunch gives a higher luminosity. It is also seen that there is no reasons for choosing different bunch lengths for the two beams; each bunch should have the bunch length as short as possible. From a consideration of the necessary RF voltages, it was decided to use 4 mm for the bunch length.

β_x at the IP	0.33	m
β_y at the IP	0.01	m
ϵ_x	1.8×10^{-8}	m
ϵ_y	3.6×10^{-10}	m
σ_z	0.004	m
(ν_x, ν_y, ν_s)	(0.52,0.08,0.017)	
Bunch population	1.4×10^{10}	electrons / bunch
	3.2×10^{10}	positrons / bunch
Total number of bunches	5120 max.	per ring

Table 3.1: Working parameter set for the half crossing angle θ_x of 11 mrad, determined from considerations on beam-beam effects, dynamic apertures and others.

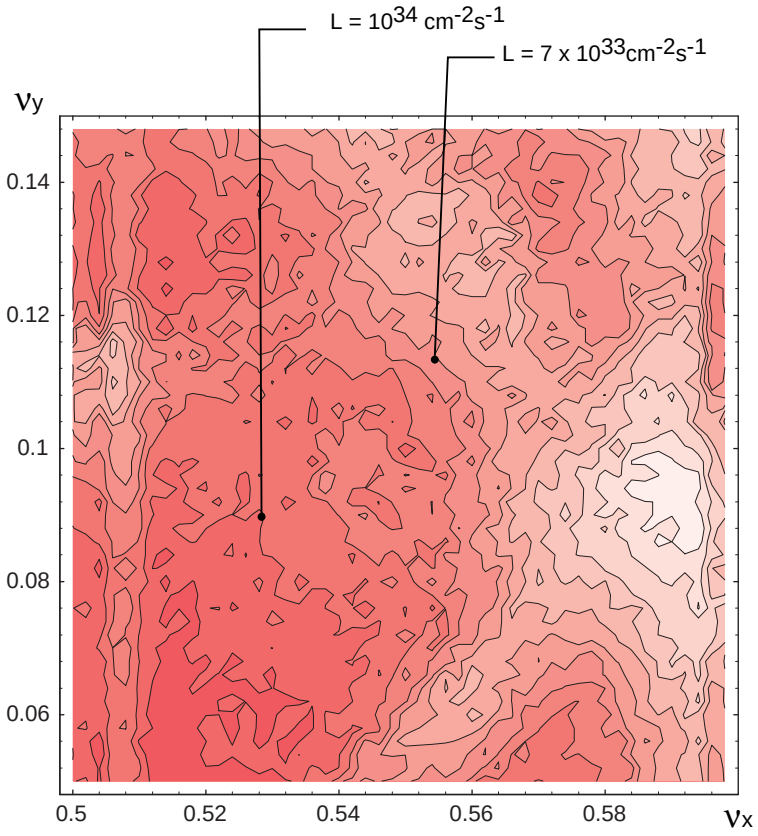

Figure 3.9: Luminosity contour diagram near the operating point.

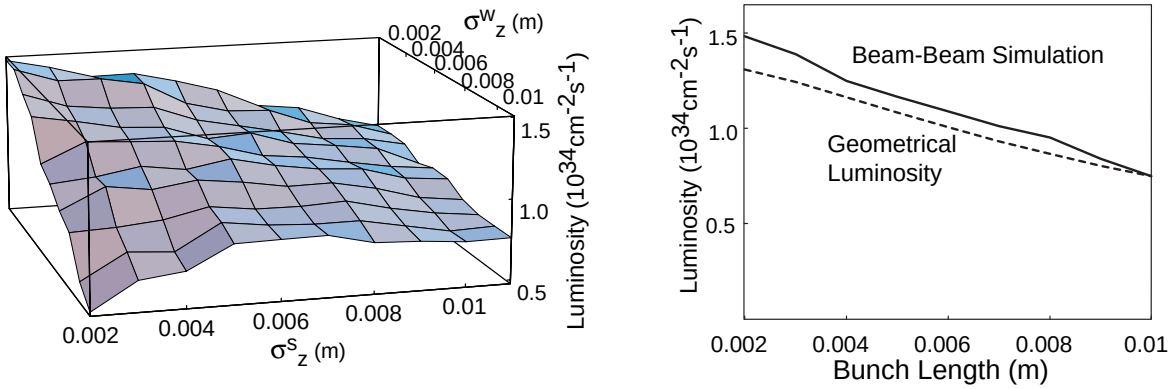

Figure 3.10: Left: Expected luminosity as a function of the bunch length (in m) of the strong bunch (σ_z^s) and the weak bunch (σ_z^w). Right: The same figure for the case with $\sigma_z^w = \sigma_z^s$.

3.4 Simulations with the Lattice Which Includes Nonlinearity and Errors

The beam-beam simulation algorithm based on the weak-strong model has been incorporated in the computer code SAD at KEK (SAD stands for"Strategic Accelerator Design" code). This facilitates a tool to study the effects of finite crossing angles at the IP, combined with the nonlinearity of the lattice and its possible errors.

3.4.1 With Quadrupole Rotation Errors Only

To create finite vertical emittance in the tracking procedure, it is necessary to assume some x-y coupling sources in the ring. As a simplified case, we first examine a nonlinear lattice where rotation errors of the quadrupole (Q) magnets are considered to be the sole source of coupling. We rotate all of the Q magnets randomly, according to

$$\text{rotation angle} = f \times \hat{r}_3,$$

where $\hat{r}_3$ is the Gaussian random variable around zero with a unit standard deviation. The distribution is cut off at 3 standard deviations. For each series of errors, we adjust f so that the σ_y equals the assumed vertical beam size at the IP. (Without errors, the vertical beam size vanishes.) A typical value of f is 5×10^{-4} rad.

Calculations of the beam-beam collision and particle tracking, now with SAD, have been conducted for up to 90,000 turns. Then, the expected luminosity is calculated. Parallel to these calculations, with the given rotation errors of the Q magnets, the single-turn beam transfer matrix with radiation damping and the single-turn diffusion

matrix of the ring are extracted[5]. These matrices are used in a beam-beam simulation with the linear ring-lattice as discussed in the previous section. The difference between the luminosity values obtained in these two methods is considered to give some information about the effects of nonlinearity in the lattice including sextupole magnets and skew fields.

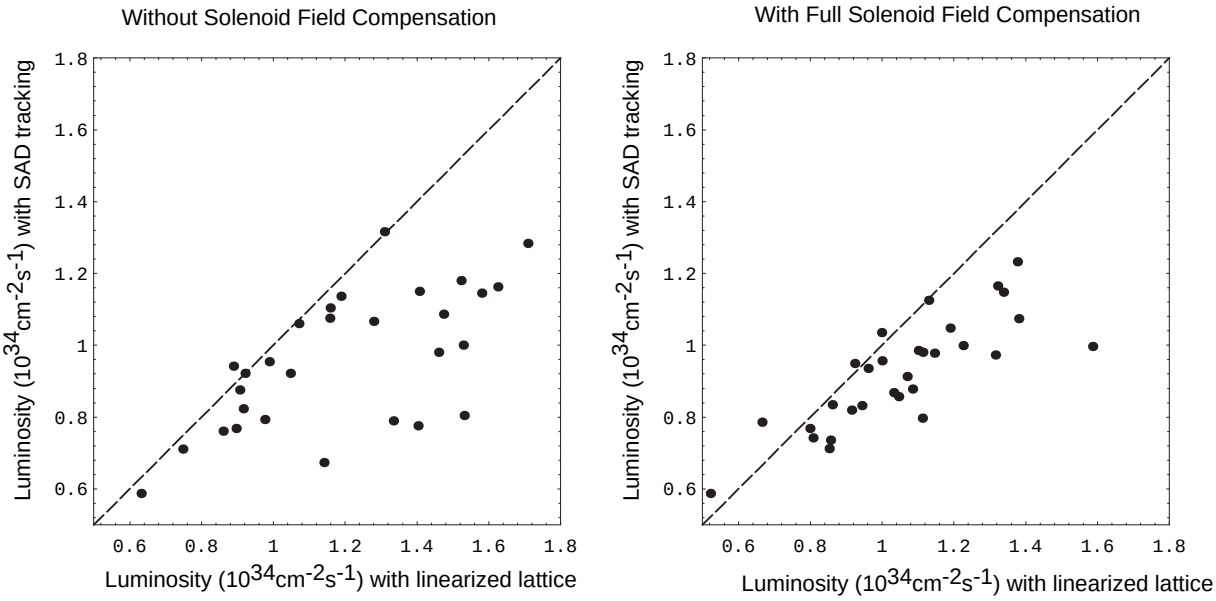

Figure 3.11: Expected luminosity in the weak-strong model calculations of beam-beam interactions, which are combined with tracking through the ring. The two diagrams show the cases where the detector solenoid field is compensated in situ at the IP (right) and without (direct) solenoid field compensations (left); the solenoid field is compensated by skew quadrupole magnets sitting at other locations.

Furthermore, to investigate the effects of the presence of a solenoid field from the experimental facility at the IP, those calculations have been repeated for two versions of the lattice design. In the first case, no explicit solenoid field compensation is made at the IP, and all of the coupling corrections are made with skew quadrupole magnets distributed in the interaction region. In the lattice case, the field compensation is achieved with counter-acting solenoid magnets.

Figure 3.11 shows the results of this study. For each data point in the scatter diagram, the horizontal coordinate gives the expected luminosity from calculations based on the linear lattice matrix. The vertical coordinate gives the luminosity expected from full SAD tracking. The diagram on the left shows the result with a lattice design which assumes no solenoid field compensation at the IP. The diagram on the right is from a lattice design with full solenoid field compensation.

The expected luminosity has been found in the range of $(0.938 \pm 0.185) \times 10^{34} \mathrm{cm}^{-2}\mathrm{s}^{-1}$, depending on the random number seed that is used to create rotation errors of quadrupole magnets. Figure 3.11 indicates that compensation of the detector solenoid field by counter-acting solenoid magnets is favored over coupling corrections with skew quadrupole magnets. The field compensation scheme at the interaction point is designed to use compensation solenoid magnets.

3.4.2 With Realistic Lattice Errors

Simulations with SAD have been repeated with a more advanced model of lattice errors. Here, finite alignment and excitation errors of the bend (B), quadrupole (Q) and sextupole (S) magnets are simultaneously considered, together with offset errors of the beam position monitors (BPMs). The typical magnitudes of the assumed errors, which we consider realistic, are summarized as follows:

type of element	BPM	B	Q	S	Steering correctors
horizontal shift (μm)	75	0	100	100	0
vertical shift (μm)	75	100	100	100	0
x-y rotation (mrad)	0	0.1	0.1	0.1	0.1
strength error	0	10^{-4}	10^{-3}	10^{-3}	0

$\times f$,

Gaussian errors ($\hat{r}_3$) are produced according to the rms values given in the table above. For each series of generated errors, orbit and tune corrections are made in the tracking code as if it were in an actual operation. Then, the scale of the assumed errors is re-normalized so that the expected vertical spot size σ_y agrees with the design value. We call this normalization factor f. With those renormalized errors in the machine, the orbit and tune corrections are, once again, performed. The expected luminosity is evaluated by using the beam-beam code, plus the tracking with SAD. Different random seeds used for generating lattice errors result in different values of f (error normalization factor) and different expected luminosity values. Some of the obtained results are:

$$\mathrm{luminosity}/10^{34}\mathrm{cm}^{-2}\mathrm{s}^{-1} = \begin{cases} 1.21 & f = 1.4 \\ 0.9 & f = 0.8 \\ 1.34 & f = 0.5 \end{cases}$$

This result indicates that the lattice nonlinearity and possible machine errors do not lead to fatal degradations of the estimated luminosity.

3.5 Quasi Strong-Strong Simulation

The results presented so far are based on a strong-weak model, where typically the HER beam (electron) is assumed to be strong, and the LER beam (positron) to be weak. To address the issues which may be overlooked in this treatment, a quasi strong-strong formalism has been developed. In this scheme, once every 500 turns of revolution the average electron and positron bunch sizes are "registered." During the next 500 turns, weak-strong model calculations are performed, while this "registered" electron (positron) bunch size is used as the "strong bunch size" for calculating the development of the positron (electron) bunch size. Then the "strong bunch sizes" are updated again, and the simulation continues.

Figure 3.12 shows the expected luminosity as a function of the revolutions. A linear lattice is used to represent the lattice beam transfer. No indications of a bunch core blow-up is seen. Figure 3.13 shows that the horizontal beam size obtained in the simulation is $\sigma_x = 6.2 \times 10^{-5}$ m. It is somewhat smaller than the nominal value 7.56×10^{-5} m. This is consistent with the dynamic beta and dynamic emittance effects.

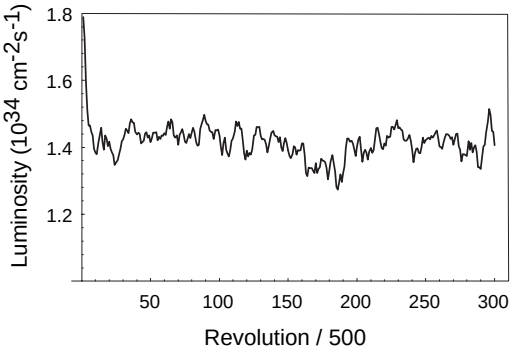

Figure 3.12: The expected luminosity as a function of the revolution number in the quasi strong-strong model calculation.

However, it has been found that unequal damping times between the LER and HER could result in unequal blow-up of the vertical tails of the two beams. This phenomenon is illustrated in Figure 3.14. There, the time development of the rms bunch size in the vertical direction for the electron (positron) is shown by solid (broken) lines. The left side represents the case where equal damping times are assumed for the LER and HER.

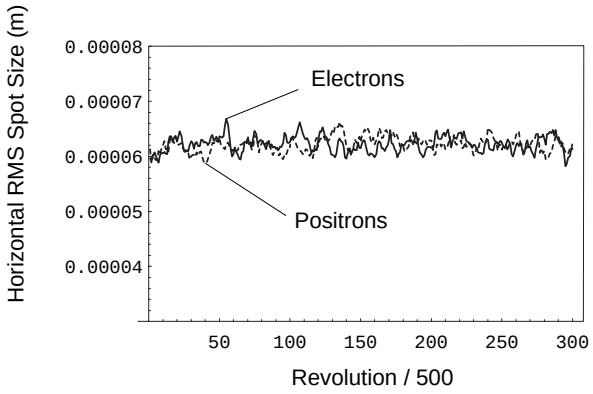

Figure 3.13: Behavior of σ_x as a function of the revolution number. The solid line shows the electron bunch size. The broken line shows the positron bunch size.

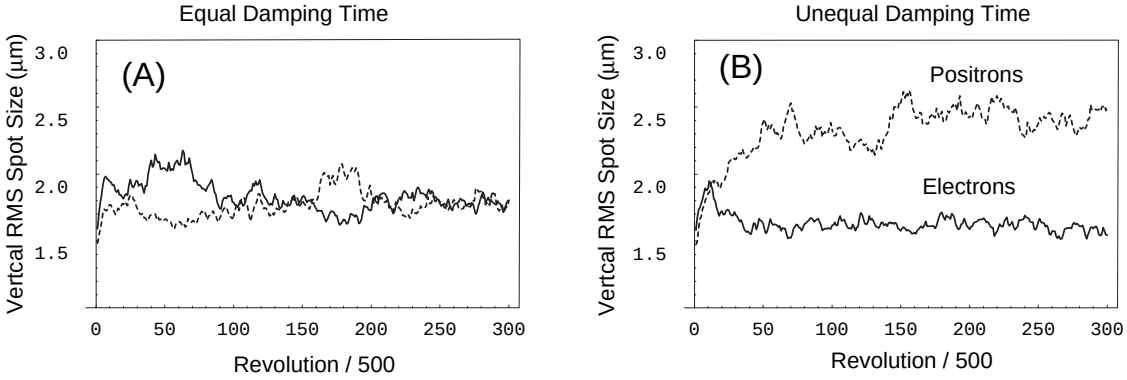

Figure 3.14: Behavior of σ_y as a function of the revolution number. The design value is $\sigma_y = 1.66 \times 10^{-6}$ m. The solid lines show the HER beam size and the broken lines show the LER beam size. The figure on the left (A) is for the case when both beams have equal damping times. Figure on the right (B) shows the case where the LER has a damping time longer by factor 2.

The right side of Figure 3.14 shows the case with unequal damping times between the LER and HER ($\tau_{\rm LER} = 2\tau_{\rm HER}$). A factor 1.5 blow-up of the positron rms size is seen. Note that the spot sizes plotted here are based on the rms of particle distributions. On the other hand, calculations of the luminosity based on the convolution of the particle distributions show no significant difference for the two cases: *i.e.* with and without equal damping times. This signature is consistent with a growth of the vertical tail. Thus, it appears desirable to maintain similar damping times for the LER and HER. This can be accomplished by using damping wigglers in the LER; it will be part of the lattice design goals.

3.6 Bunch Tails Excited by Beam-Beam Interactions

The presence of non-Gaussian bunch tails causes an extra synchrotron radiation (SR) background to the detector facility, which is harmful to its data collection and data analysis. The fractional bunch tail population should be kept less than 10^{-5} for $> 10\sigma_x$ and 10^{-5} for $> 30\sigma_y$, according to design considerations on SR masks near the interaction point.

The development of bunch tails due to beam-beam interactions has been studied with a long-term strong-weak calculation with a linear lattice model. Typically the simulation is done by tracking 50 super particles over 10^8 turns of revolution. This means 1000 seconds for 50 particles, and 14 hours for a single particle in the actual machine.

Figure 3.15 shows the calculated particle distribution as a function of the action variable I_y in the vertical coordinate,

$$I_y = \frac{1}{2}\left[y^2/(\sigma_y)^2 + p_y^2/(\sigma_{p_y})^2\right]. \tag{3.1}$$

The particle distribution function $\rho(I_y)$ is normalized to unity. In Figure 3.15 the vertical axis indicates $\log_{10}(\rho(I_y))$. The core part is identical with the nominal Gaussian distribution. Non-gaussian tails in the particle distribution are seen. In this case the function $\rho(I_y)$ can be fitted with a sum of

$$\rho(I_y) \lesssim e^{-I_y} + 5.2\times 10^{-3} e^{-0.15 I_y} + 3\times 10^{-6} e^{-0.04 I_y}. \tag{3.2}$$

We define the normalized vertical amplitude A_y as

$$A_y = \sqrt{2I_y}.$$

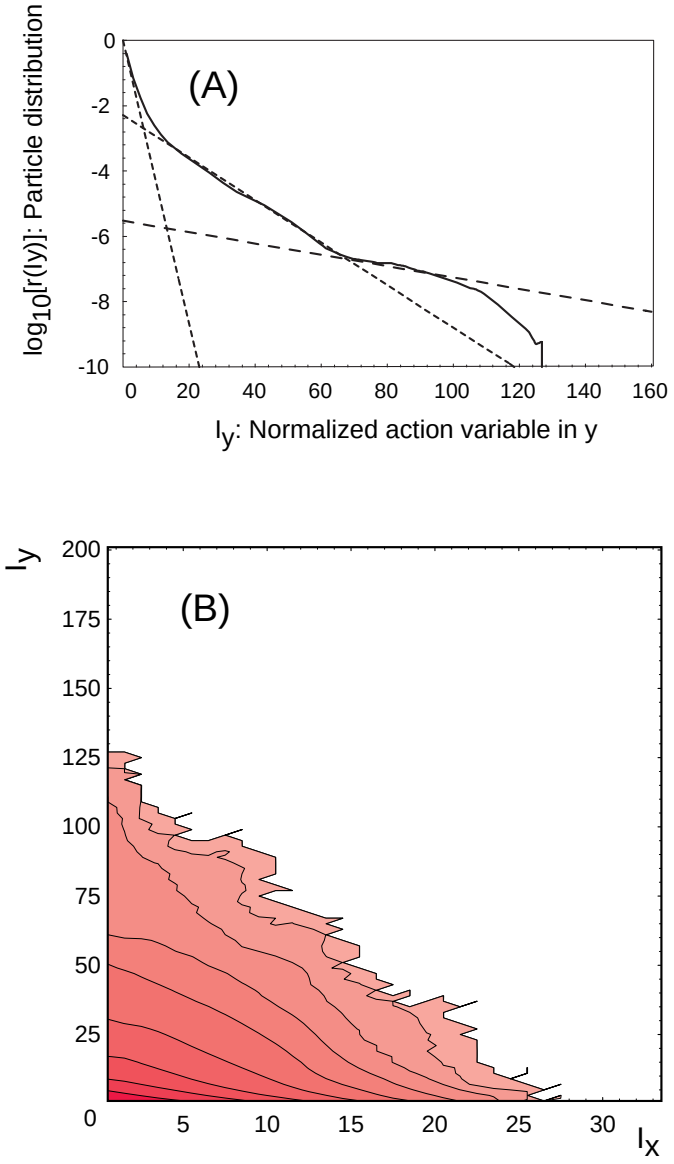

Figure 3.15: (A) Tail distribution for an ideal linear lattice as a function of the normalized nominal action I_y. (B) The same distribution in the (I_x, I_y) space. The contour lines are drawn for each factor step of 10.

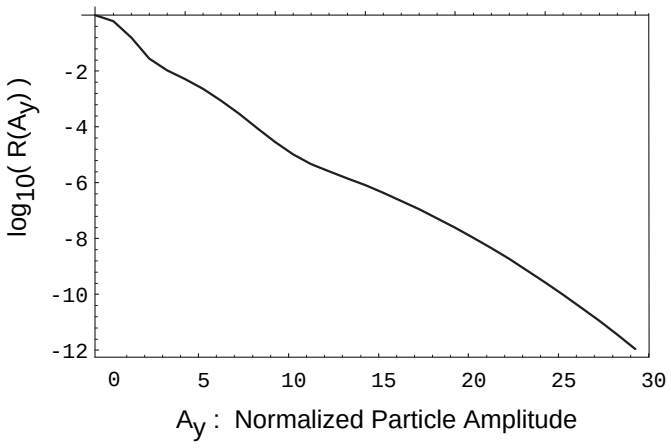

Figure 3.16: Probability of a particle having the amplitude larger than A_y.

Then the probability of finding a particle whose amplitude exceeds A_y is calculated as

$$R[A_y] = \int_{A_y}^{\infty} \rho(I_y) A_y dA_y.$$

Figure 3.16 shows $\log_{10}(R[A_y])$ as a function of A_y, based on the calculations shown in Figure 3.15.

It can be seen that the probability that a particle has a vertical amplitude larger than $30\sigma_y$, where σ_y is the design bunch size, is approximately 10^{-12}. Since the bunch population is on the order of 10^{10}, no particle is likely to have such a large vertical amplitude. Tails in the horizontal direction have been also studied. It has been found that the development of horizontal bunch tails is much slower than in the vertical direction. The limit imposed by requirements on the small synchrotron radiation background to the detector facility is satisfied without problems. Preparations are under way to evaluate bunch tails by using tracking calculations which include non-linear effects of the lattice and possible machine errors.

3.7 Tail, Luminosity and Longitudinal Tilt

The dependence of the tail behaviors on the tunes have been studied. To characterize the size of bunch tails the largest amplitude (a_x, a_y) among 50 super-particles during several damping times is picked up. The part (A) and (B) of Figure 3.17 show luminosity contour plots for the region $0.5 < \nu_x < 1.0$ and $0 < \nu_y < 0.5$ along with the maximum particle amplitude in the vertical direction. They show that luminosity reduction is frequently associated with a growth of vertical tails, but not necessarily so all the time.

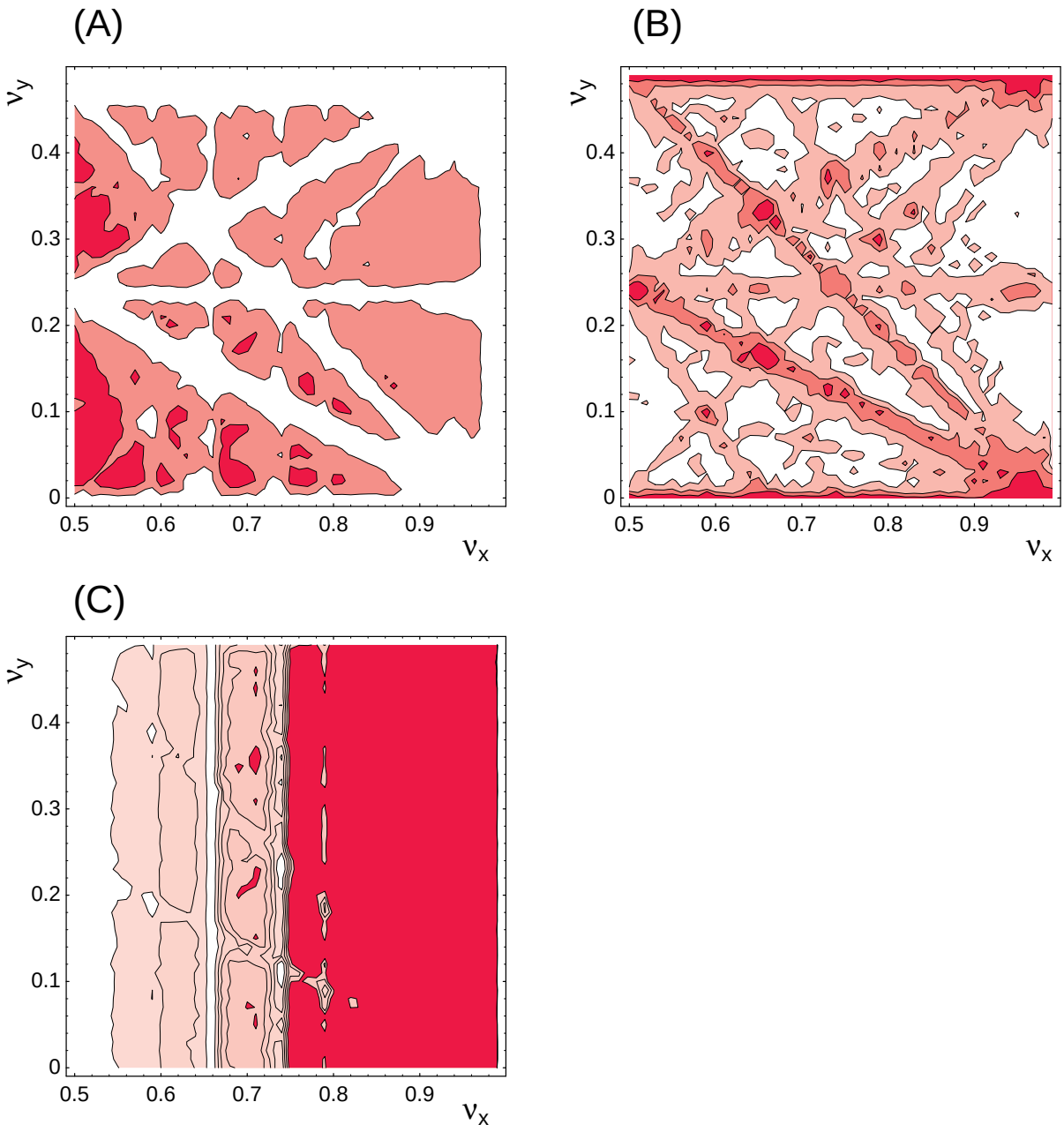

Figure 3.17: (A) Luminosity contour diagram in the ν_x-ν_y plane. The contour lines are drawn for luminosity values of 10^{34} and 0.5×10^{34} cm^{-2}s^{-1}. (B) Contour diagram of the maximum vertical amplitude of bunch particles. Contour lines are drawn for $30\sigma_{0y}$, $20\sigma_{0y}$ and $10\sigma_{0y}$, where σ_{0y} is the nominal vertcal beam size. (C) The longitudinal tilt angle ϕ_{xz} is shown. The contour lines are drawn for 1, 0.8, 0.6, 0.4,and 0.2 mrad.

The angle of the beam envelope relative to the longitudinal coordinate has been also calculated at the same time. The crossing angle in the collision introduces a coupling between the transverse and longitudinal coordinates. Consequently, the principal axes of the bunch may tilt not only transversely, but also longitudinally. We calculate the longitudinal tilt angle in the head-on frame as

$$\phi_{xz} = \frac{1}{2}\arctan\left\{\frac{2\langle xz\rangle}{\langle zz\rangle - \langle xx\rangle}\right\} - \theta_x.$$

Here, $\langle xz\rangle$ represents the long term (three damping times) average of xz. Similar definitions hold for $\langle xz\rangle$ and $\langle xx\rangle$. To be more precise, evaluation should be made with a strong-strong model simulation. However, the weak-strong results can indicate how serious the effect is.

Part (C) of Figure 3.17 shows a contour diagram of the calculated ϕ_{xy}. The longitudinal tilt angle increases as ν_x approaches the integral value from below. It exceeds 1 mrad for $\nu_x > 0.75$.

3.8 Summary of Beam-Beam Simulations with Finite Crossing Angles

The estimated values of the luminosity in the simulations presented so far are summarized in Table 3.2. The assumed beam parameters are set as in Table 3.1.

Method	Luminosity ($\times 10^{34}$)	Legend
1	1.16	Geometrical
2	1.24	Ideal linear lattice
3	0.938±0.185	Nonlinear lattice
4	0.9 to 1.34	Nonlinear lattice with realistic errors and corrections
5	1.4	Quasi strong-strong (equal damping)

Table 3.2: Comparison of the expected luminosity values evaluated by various simulations.

Brief descriptions of individual cases in Table 3.2 are given bellow:

1. Expected luminosity with the 2×11 mrad crossing angle, where only the geometric effects are considered. Dynamical effects, such as the dynamic beta and dynamic emittance, are not considered.

2. Weak-strong beam-beam simulation, combined with a linear, error-free lattice.

3. Weak-strong beam-beam simulation, combined with a nonlinear lattice. Rotation errors of the Q magnets are used to create the finite luminosity coupling. The variations are due to the difference in the seed used to generate the rotation errors. Full compensation of the detector solenoid field is assumed.

4. Weak-strong beam-beam simulation, combined with the nonlinear lattice model. Excitation and alignment errors of bend, quadrupole and sextupole magnets are considered. Orbit and coupling corrections are performed in the tracking code, mimicking the actual operation.

5. Quasi strong-strong simulation with a linear, error-free lattice. Equal damping times for the HER and LER are assumed.

It is seen that within the simulation studies conducted so far, the luminosity in the design goal can be achieved with a finite angle crossing of 2×11 mrad at the interaction point. Unfortunately, this performance cannot be fully experimentally tested until operating the real-life KEKB machine. As a back-up safety measure, the use of crab crossing scheme to combine with the finite angle collision is being considered. The status of its R&D efforts is presented in Chapter 8. Meanwhile, more elaborate studies of beam-beam effects will be continued:

- In a tail simulation, nonlinear effects in the lattice should be included in the calculation.

- In a weak-strong simulation with a nonlinear lattice, error correction schemes from the beam-beam point of view will be examined.

- The strong-strong simulation will be updated so that it can evaluate the beam envelopes in each turn, using a Gaussian approximation to calculate the beam-beam forces.

- A more ambitious strong-strong simulation which does not rely on the Gaussian approximation to calculate the beam-beam force is being developed.

One example of storage rings which implemented a finite crossing angle in the past is DORIS at DESY. It has been known that difficulties were encountered in its operation. According to a report [2]:

"Although the width of these satellite resonances (due to synchro-betatron resonances) is very small (< 0.001) as compared to the distance between the resonances,

they limit the luminosity of the storage ring DORIS. The reasons are the decoupling transmitter and the rf-quadrupole, which are needed to suppress instabilities. The decoupling transmitter gives to different bunches different synchrotron frequencies, with a spread of $\Delta Q_s = \pm 0.006$. The rf-quadrupole produces a spread in betatron frequencies of $\Delta Q_\beta = \pm 0.005$. At the present operating point between 6.24 and 6.15, there are always some bunches on a resonance."

"The theoretical and experimental investigations have shown that the satellite resonances are weaker for Q_β-values closer to an integer. We therefore expect that shifting the operating point into a region near 6.1 will permit higher currents and thus increase the luminosity."

Attention has been paid in the KEKB design so that those conditions which could lead to serious operational difficulties will be avoided. For instance, a fairly low synchrotron tune ($0.01 < \nu_s < 0.02$) will be used. The coupled-bunch instabilities will be addressed by careful design of the RF cavities, feedback systems and an optimized choice of operating parameters, and by not introducing a tune spread.

3.9 Comments on Parasitic Crossing Effects

When the half crossing angle is small ($\sim$ a few mrad or less), the issue of parasitic crossing is quite difficult to study theoretically. This is because both the focussing effects and shifts of bunch centroid need to be considered in a multi-bunch, multi-crossing condition in a 3-dimensional way. Studies have been carried out with simulation calculations for a bunch spacing as small as 0.6 m:

1. A strong-strong model simulation based on the Rigid Gaussian Model has been conducted. Closed orbit effects due to parasitic collisions have been analyzed. It was observed that the closed orbits of individual bunches will differ from each other for a smaller (a few mrad or less) crossing angle. In extreme cases, a closed orbit may not exist at all. Chaotic behaviors of clusters of bunches can result, having orbit deviations exceeding $10\sigma_x$.

2. A 2-dimensional weak-strong model simulation to analyze the beam size during injection and collision conditions has been performed. It was found that for small crossing angles, the injected beam can rapidly blow up, exceeding the dynamic aperture limit, and may never become damped to acceptable sizes.

However, it should be pointed out that the validity of the results for small crossing angles ($<$ a few mrad) with a small bunch spacing ($<$ 1 m) are limited by the approxi-

mation which is used in the simulation. With the present-day capabilities of computing facilities, it appears to be very difficult to obtain reliable results in a realistic computation time. Thus, for a crossing angle $< 2 \times 2.5$ mrad, exact statements cannot be made, except that the acceptable bunch spacing is likely to be limited to roughly 3 m or larger.

Fortunately, the choice of a 11×2 mrad crossing allows us to evaluate the effects of parasitic collisions with an approximation that is based on the simplified Gaussian model with adequate accuracies. This is because the beam separation at the first and subsequent parasitic crossing points will be large (> 6 mm), and the forces between opposing bunches in parasitic crossing will be quite weak. No fatal effects have been observed for a half crossing angle near 10 mrad in weak-strong or strong-strong simulations. We consider that it is safe to conclude that the effects of parasitic collisions at KEKB with a crossing angle of 2×11 mrad are negligible.

Bibliography

[1] For a treatment of the beam-beam interaction, see K. Hirata, H. Moshammer and F. Ruggiero, Particle Accelerators **40**, 205 (1993); K. Hirata, Phys. Rev. Lett., **74** 2228(1995); N. Toge and K. Hirata, *Study on Beam-Beam Interactions for KEKB*, KEK Preprint 94-160 (1994).

[2] A. Piwinski, IEEE Trans. on Nucl. Sci. **24** 1408 (1977).

[3] B. Richter, Proc. Int. Sym. Electron and Positron Storage Rings, Saclay, 1966.

[4] K. Hirata and F. Ruggiero, Particle Accelerators **28**, 137 (1990). (Proceedings of XIV Int. Conf. on High Energy Accel. 1989 Tsukuba.)

[5] K. Ohmi, K. Hirata and K. Oide, Phys. Rev. **E49**751(1994).